AEM
Journals.ASM.org

Structural and Mechanistic Insights into the *Pseudomonas fluorescens* 2-Nitrobenzoate 2-Nitroreductase NbaA

Yong-Hak Kim,[a] Wooseok Song,[a] Jin-Sik Kim,[b] Li Jiao,[c] Kangseok Lee,[d] Nam-Chul Ha[b]

Department of Microbiology, Catholic University of Daegu School of Medicine, Daegu, Republic of Korea[a]; Department of Agricultural Biotechnology, Center for Food Safety and Toxicology, Center for Food and Bioconvergence, Research Institute for Agriculture and Life Sciences, Seoul National University, Seoul, Republic of Korea[b]; Department of Manufacturing Pharmacy, Pusan National University, Busan, Republic of Korea[c]; Department of Life Science, Chung-Ang University, Seoul, Republic of Korea[d]

The bacterial 2-nitroreductase NbaA is the primary enzyme initiating the degradation of 2-nitrobenzoate (2-NBA), and its activity is controlled by posttranslational modifications. To date, the structure of NbaA remains to be elucidated. In this study, the crystal structure of a Cys194Ala NbaA mutant was determined to a 1.7-Å resolution. The substrate analog 2-NBA methyl ester was used to decipher the substrate binding site by inhibition of the wild-type NbaA protein. Tandem mass spectrometry showed that 2-NBA methyl ester produced a 2-NBA ester bond at the Tyr193 residue in the wild-type NbaA but not residues in the Tyr193Phe mutant. Moreover, covalent binding of the 2-NBA methyl ester to Tyr193 reduced the reactivity of the Cys194 residue on the peptide link. The Tyr193 hydroxyl group was shown to be essential for enzyme catalysis, as a Tyr193Phe mutant resulted in fast dissociation of flavin mononucleotide (FMN) from the protein with the reduced reactivity of Cys194. FMN binding to NbaA varied with solution NaCl concentration, which was related to the catalytic activity but not to cysteine reactivity. These observations suggest that the Cys194 reactivity is negatively affected by a posttranslational modification of the adjacent Tyr193 residue, which interacts with FMN and the substrate in the NbaA catalytic site.

Many nitroaromatic compounds present as environmental pollutants and drugs cause mutagenic and cytotoxic effects in mammals. These compounds are likely to undergo reductive activation by cellular enzymes such as thioredoxin reductase, generating superoxide and leading to reactive oxygen species (ROS)-induced oxidative stress, a major mechanism of cytotoxicity (1). In bacteria, nitroaromatic compounds are degraded to less toxic or nontoxic metabolites by oxidative or reductive enzymes, which are able to release nitrite (NO_2) from the aromatic ring or reduce the nitro group to hydroxylamine (2, 3). Bacterial reduction of the nitro group to hydroxylamine is similar to that seen in mammals but differs with respect to the high catalytic efficiency and oxygen insensitivity of bacterial nitroreductases, which do not readily transfer one electron to molecular oxygen to generate the superoxide radical. In addition, some prokaryotic and eukaryotic reductases are capable of releasing nitrite through the formation of a hybrid-Meisenheimer complex of the nitroaromatic ring (4).

Bacterial degradation of nitrobenzoate (NBA) is important for the mineralization of nitroaromatic compounds to nontoxic end products. Since the first isolation of bacterial strains with the ability to use 2- or 4-NBA as the sole carbon, nitrogen, and energy source in the late 1950s (5), a few strains with catabolic genes have been identified. Among them, *Pseudomonas fluorescens* KU-7 has been extensively studied for the entire degradation pathways of 2-NBA, encoded in the *nbaYAB* (6) and *nbaEXHJIGFCDR* (7) operons. In the upper pathway, 2-nitroreductase (NbaA) plays a key role in the reduction of 2-NBA to 2-hydroxylaminobenzoate, which is then transformed to 3-hydroxyanthranilate (3-HAA) by the mutase NbaB. The lower pathway, which attacks 3-HAA via ring cleavage (NbaC), decarboxylation (NbaD), and further conversions to yield acetyl coenzyme A (acetyl-CoA), is homologous to the degradation of 2-aminophenol in *Pseudomonas* sp. strain AP-3 (8). In *Pseudomonas putida* TW3, the key step of reducing 4-NBA to 4-hydroxylaminobenzoate is achieved by 4-nitroreductase (PnbA) followed by deaminase activity (PnbB) to produce ammonia and protocatechuate, which is degraded through the β-ketoadipate pathway (9). However, there is no report of a reductive pathway for 3-NBA; instead, 3-NBA is oxidized to protocatechuate with the release of nitrite by an aromatic ring 3,4-dioxygenase, such as MnbA in *Comamonas* sp. strain JS46 (10). Because the reactivity of NBA isomers is analogous to that of benzoic acid but with a substitution of the nitro group, the 2- and 4-nitro groups, but not the 3-nitro group, easily accept electrons transferred by regioselective nitroreductases.

Among the various NBA metabolites, 3-HAA represents an alternative pathway for 2-NBA degradation through a Bamberger-like rearrangement of 2-hydroxylaminobenzoate that is otherwise degradable in the deamination process of anthranilate (11, 12). 3-HAA is also naturally produced via the degradation of L-tryptophan through the kynurenine pathway, with important neuropsychiatric implications (13). It is likely that bacterial 3-HAA synthesis, if safer and more efficient than chemical synthesis (14), will benefit the development of pharmaceutical agents active against

Received 19 April 2015 **Accepted** 20 May 2015

Accepted manuscript posted online 29 May 2015

Citation Kim Y-H, Song W, Kim J-S, Jiao L, Lee K, Ha N-C. 2015. Structural and mechanistic insights into the *Pseudomonas fluorescens* 2-nitrobenzoate 2-nitroreductase NbaA. Appl Environ Microbiol 81:5266–5277. doi:10.1128/AEM.01289-15.

Editor: R. E. Parales

Address correspondence to Yong-Hak Kim, ykim@cu.ac.kr, or Nam-Chul Ha, hanc210@snu.ac.kr.

Supplemental material for this article may be found at http://dx.doi.org/10.1128/AEM.01289-15.

doi:10.1128/AEM.01289-15

the 3,4-dioxygenases associated with human and animal brain diseases (15, 16). It has been shown that the *nbaAB* system, when expressed in *Escherichia coli* lacking the activity for degradation of 2-aminobenzoate and 3-HAA, is not as effective in reducing 2-NBA as expected based on *in vitro* enzyme assays (6). Recombinant *E. coli* cells are able to stimulate the generation of H_2O_2, causing alterations in enzyme activity and substrate specificity, leading to enzyme inactivation through the formation of intermolecular disulfide bonds (17, 18). However, the H_2O_2 effect is not sufficient to explain why NbaA activity is much lower under reduced cytoplasmic conditions than under the oxidized *in vitro* condition.

In this study, we aimed to obtain the crystal structure of an NbaA variant with substitution of alanine for cysteine 194 (Cys194Ala) and identify the catalytic site where inhibition occurs in the reduced as well as in the oxidized form. The wild-type NbaA was difficult to crystallize using conventional methods, even when using a high concentration of a reducing agent, presumably because of the intermolecular disulfide bonds between the two reactive Cys141 and Cys194 residues. However, the Cys194Ala variant of NbaA was readily crystallized without apparent change to the catalyzed reaction. In order to obtain structural information on the substrate binding site in the wild-type NbaA, the 2-NBA methyl ester substrate-analog inhibitor was covalently bound to active site and was identified by tandem mass spectrometry. Based on this data, site-directed mutant analysis was conducted to examine the role of a modified amino acid residue in the NbaA catalytic site. We presented here that the hydroxyl group of tyrosine 193 (Tyr193) in NbaA was modified through a transesterification reaction with the 2-NBA methyl ester, thereby resulting in enzyme inactivation due to the release of a flavin (flavin mononucleotide [FMN]) cofactor from the catalytic site.

MATERIALS AND METHODS

Materials and chemicals. The following chemicals were purchased from Sigma (St. Louis, MO): 5,5′-dithio *bis*-(2-nitrobenzoic acid) (DTNB), dithiothreitol (DTT), iodoacetamid, isopropyl-β-D-thiogalactopyranoside (IPTG), NADPH, 2-nitrobenzoic acid (2-NBA), 2-nitrobenzoate methyl ester, and riboflavin 5′-monophosphate (FMN) sodium salt dehydrate. The fast protein liquid chromatography system and column resins were purchased from GE Healthcare Life Science (Uppsala, Sweden), and sequencing-grade chymotrypsin and trypsin were obtained from Roche (Mannheim, Germany) and Promega (Madison, WI), respectively. Other solvents and reagents used were of analytical grade and were obtained from USB Corporation (Cleveland, OH), J. T. Baker (Phillipsburg, NJ), and Merck (Darmstadt, Germany).

Strains and culture conditions. The *nbaA* gene was cloned into pSD80, and the resulting pNbaA plasmid was used as a template to construct a mutant *nbaA* gene encoding the Cys194Ala change by primer extension PCR as described elsewhere (17). To examine the Tyr193 functional group modified by 2-NBA methyl ester, a tyrosine 193-to-phenylalanine (Tyr193Phe) site-directed mutant gene was constructed in both the pNbaA and Cys194Ala mutant plasmids using the pSD80 primers (pSD80F, 5′-GAGCTGTTGACAATTAAT, and pSD80R, 5′-AGGACG GGTCACACGCGC) and *nbaA*-specific primers (Y193F-F, 5′-GGCG CTTGGGAGGACCCAACTTTTGCCGAACCACCGACCGGGTTC, and NbaA-557R, 5′-AGTTGGGTCCTCCCAGCGCC), which changed the UAU codon for Tyr193 to the UUU codon for phenylalanine at the underlined sequence. All recombinant constructs were confirmed by DNA sequencing. The resultant plasmids were used to transform *Escherichia coli* strain BL21(DE3) and were induced by the addition of 0.1 mM IPTG to an exponentially growing cell suspension (approximate optical density at 600 nm [OD_{600}] = 0.5) in LB medium at 37°C with shaking at 180 rpm.

Protein purification. Wild-type NbaA and mutant proteins that were overproduced in *E. coli* were routinely purified by fast protein liquid chromatography at 4°C. Harvested cells were resuspended in lysis buffer containing 20 mM Tris-HCl (pH 8.0), 150 mM NaCl, and 10 mM 2-mercaptoethanol. Cells were disrupted by sonication, and debris was removed by centrifugation. The supernatant was loaded onto a DEAE-Sepharose column that was equilibrated with loading buffer containing 20 mM Tris-HCl (pH 8.0) and 10 mM 2-mercaptoethanol. The protein was eluted by a linear gradient of 0 to 1 M NaCl in loading buffer. Fractions containing wild-type or mutant NbaA protein were pooled and treated with 1 M ammonium sulfate. The protein was loaded onto a phenyl-Sepharose column that was equilibrated with 1 M ammonium sulfate, and eluted by a linear gradient of the loading buffer. The collected wild type and mutant NbaA apoprotein fractions were concentrated using Centriprep filter units (Millipore Co., Bedford, MA). The concentrated proteins were reconstituted by the addition of 1 mM FMN and 1 mM $MnCl_2$, further purified using a HiLoad Superdex 200 column (GE Healthcare, Milwaukee, WI), and concentrated using Centriprep filter units at a concentration of 20 mg ml^{-1} in lysis buffer. Protein concentration was determined using a Bradford reagent (Bio-Rad, USA). The final purified protein samples were stored at −80°C until use. If necessary, buffers were exchanged using PD10 desalting columns.

Crystallization, data collection, and structural determination. It was difficult to obtain a crystal of the wild-type NbaA using multiple conventional methods, even in the presence of a high concentration of a reducing agent (5 mM DTT or 10 mM mercaptoethanol), because of distorted protein structure in the solution. Therefore, the Cys194Ala mutant protein, which decreased the extent and progression of disulfide formation without an apparent change in catalysis (18), was used for crystallization in a precipitation solution containing 0.1 M sodium acetate (pH 4.6), 1 mM FMN, 1 mM $MnCl_2$, and 30% (vol/vol) polyethylene glycol 4000 (PEG 4000) at 14°C. X-ray diffraction data for the crystals were collected on beamline 5C at the Pohang Accelerator Laboratory (PAL, Pohang, Republic of Korea) using a Quantum 315 CCD detector (ADSC). The diffraction data sets were handled and scaled using the HKL2000 package (19). The crystal belongs to the $P6_4$ space group with the following cell dimensions: a = 70.5 Å, b = 70.5 Å, and c = 80.4 Å. Initial phases were determined by the molecular replacement package MOLREP (20) using the coordinates of FMN-binding protein from *Methanothermobacter thermautotrophicus* (PDB code 1EJE) as a search model (21). Model building was performed with Coot (22), and model refinement was conducted using the program PHENIX (23).

Enzyme inhibition. The inhibitory effects of various DTNB and 2-NBA methyl ester concentrations on the FMN-reconstituted NbaA were analyzed in 20 mM sodium phosphate buffer (pH 7.4) under ambient conditions. After a 10-min preincubation of inhibitor-treated samples on ice, soluble inhibitor was removed using PD10 desalting columns in order to examine the recovery of enzyme activity. Enzyme activity was assayed by the addition of 1 mM 2-NBA to 20 mM sodium phosphate buffer (pH 7.4) containing a 0.1 μM monomer concentration of NbaA, 1 mM NADPH, 10 μM FMN, and 0.1 mM $MnCl_2$ at room temperature. The rate of NADPH oxidation was measured at 340 nm (ε = 6.21 mM^{-1} cm^{-1}) using a Shimazu UV-1800 spectrophotometer (Shimazu Co., Kyoto, Japan) installed with UVProbe version 2.33 software.

Measurements of FMN content and cysteine reactivity. Using FMN-reconstituted dimers purified by gel filtration, FMN contents of the wild-type and mutant NbaA were determined by a spectrophotometric method (24). Briefly, absorbance spectra of FMN-reconstituted dimers were recorded between 300 nm and 500 nm at 0.5-nm intervals. After treatment with 0.2% SDS, tightly sealed sample tubes were boiled for 10 min so as to release FMN from protein. The released FMN concentration was measured by the extinction coefficient of FMN (ε = 12,200 M^{-1} cm^{-1}) at 446 nm (25). To determine the protein concentration, bound FMN was com-

pletely removed from the gel-filtered samples by the addition of trichloroacetic acid (TCA; 10%, wt/vol). After centrifugation, the precipitates were washed twice with cold 80% acetone and air-dried pellets were dissolved by boiling in the same buffer containing 0.2% SDS. The concentration of NbaA homodimer was determined by the calculated extinction coefficient of 46 mM^{-1} cm^{-1} at 280 nm. To investigate the effects of NaCl concentration on FMN content and cysteine reactivity of wild-type NbaA, the apoprotein was reconstituted with 1 M FMN and 0.1 mM $MnCl_2$ in 20 mM sodium phosphate (pH 7.4) buffer containing 0.1 M, 0.35 M, 0.45 M, or 0.55 M NaCl and the homodimeric protein was purified by gel filtration using the same buffers. Enzymatic activity of the FMN-reconstituted dimer was measured by mixing 1 mM 2-NBA and 1 mM NADPH in the same buffers. After treatment of the purified proteins with 10 mM iodoacetamide for 1 h at room temperature in the dark, nondenaturing SDS-PAGE was performed to analyze the patterns of disulfide bonding, and the excised monomer bands were analyzed by nanoflow liquid chromatography (nLC)-tandem mass spectrometry (MS/MS).

MS. For disulfide bond analysis, 1 μg of trypsin-digested protein solution was repeatedly analyzed by a Thermo LTQ-Velos mass analyzer equipped with a reversed-phase Magic C18AQ capillary column (75-μm inner diameter by 360-μm outer diameter by 7-cm length) and an EASY-nLC 1000 pump system, with delivery at a constant rate of 300 nl min^{-1}. The chromatographic conditions were a 90-min linear gradient from 5% to 40% acetonitrile in 0.1% formic acid solution, followed by a 10-min column wash with 80% acetonitrile and 20 min of reequilibration to the initial buffer solution. Survey full-scan MS spectra were acquired between *m/z* 300 and 2,000, and MS/MS spectra of the five most intense ions from the preview survey scan were acquired in the ion trap with the following settings: isolation width, ±1.5 *m/z*; collision energy, 35%; and dynamic exclusion duration, 30 s. The top-ranked MS2 precursor ions and tandem mass spectra were analyzed using Thermo Proteome Discoverer program version 1.3 using a database of NbaA protein (GenBank accession number BAF56676.1), *E. coli* proteins, and common contaminants obtained from the Swiss-Prot/UniProtKB (http://www.uniprot.org) and the Max Planck Institute of Biochemistry, Martinsried (http://maxquant.org/contaminants.zip). The number of tandem mass spectra that matched to disulfide-bonded peptides was determined using an in-house Excel macro program with the following settings: average mass (*m/z*) of tryptic peptide; precursor ion mass tolerance, 0.8 Da; fragment mass tolerance, 1 Da; and disulfide bond formation with a loss of two protons (−2.016 Da) between the two tryptic peptides, each containing cysteine.

For identification and quantification of peptides modified by 2-NBA methyl ester or iodoacetamide, monomer bands of wild-type NbaA and the Tyr193Phe mutant were isolated from nondenaturing SDS-PAGE gels digested with both trypsin and chymotrypsin in order to improve the elution and detection rate of the modified peptide(s) from the nLC-tandem mass spectrometry, as described previously (26). All samples were prepared under N_2 gas and stored in dark vials at 4°C to avoid artifacts that arise from cysteine oxidation. The SEQUEST search options were average mass (*m/z*); maximal 1 miscleavage site of trypsin and chymotrypsin; precursor ion mass tolerance, 0.8 Da; fragment mass tolerance, 1 Da; iodoacetamide modification of cysteine (57.02 Da); and transesterification (149.01 Da) of 2-NBA methyl ester at the hydroxyl group of serine, threonine, or tyrosine. Tandem mass spectrometry data were obtained after filtering out with a probability of >99% and a target-decoy false-discovery rate (FDR) of <0.01. Relative intensities of the peptides eluted within the retention time of 1.5 min were calculated using extracted ion chromatograms normalized to the intensity of an unmodified peptide, DLTPSTTIDVPR (m/z = 658.23, z = +2), which was used as an internal standard.

RESULTS

Structural determination of NbaA. NbaA from *P. fluorescens* consists of 216 amino acid residues and has a molecular mass of ~24 kDa. The full-length protein was overproduced in *E. coli* and purified to homogeneity using conventional chromatographic techniques. Unfortunately, we failed to obtain any protein crystals with the wild-type protein despite extensive screening and troubleshooting after crystallization conditions. We thought that crystallization might be hampered by the formation of intermolecular disulfide bonds mediated by Cys141 and Cys194. To mitigate the disulfide bond formation, the Cys194 residue, which is not conserved among NbaA homologs, was replaced with alanine. Using an FMN-reconstituted protein of the Cys194Ala mutant, we successfully obtained yellow crystals with a hexagonal bipyramidal shape using the hanging drop method at 14°C and pH 4.6 (see Fig. S1 in the supplemental material). The crystal structure of the Cys194Ala mutant was determined by the molecular replacement method using an FMN-binding protein (PDB code 1EJE) of *M. thermautotrophicus* as a search model (21). The crystal structure belonged to the $P6_4$ space group with a single molecule (a protomer) in the asymmetric unit. The final model was refined to a 1.7-Å resolution, containing all of residues 2 to 213 with the exception of residues 64 to 73, which were disordered in the crystal (Fig. 1). The structure was refined to a free *R* value of 22.5% with good stereochemistry. Further details on the structure determination and refinement are given in Table 1.

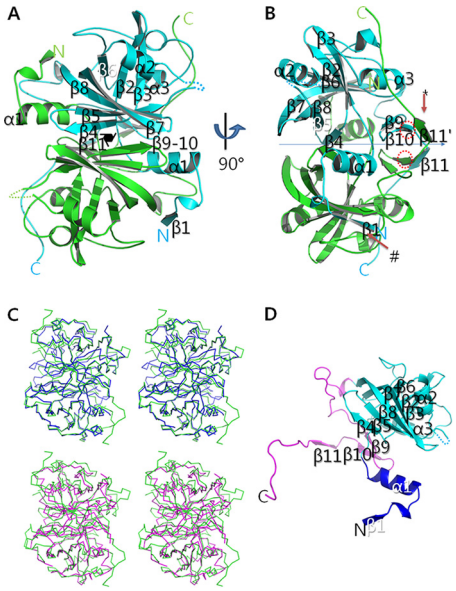

FIG 1 Overall structure of NbaA. (A and B) Ribbon diagrams of the NbaA dimer showing two orthogonal views. The protomers are colored in cyan or green. The c-axis with 6_4-fold symmetry is normal to the plane of projection (A) or parallel to the plane of projection (B). The c-axis is displayed as a graphic symbol of the 6_4-fold symmetry (A) or as a black line (B). The asterisk and pound sign mark indicate the interprotomer interactions mediated by hydrogen bonding between the backbones. The red circles in broken lines indicate β10 containing Tyr193 and Cys194 (B). (C) Stereo diagrams representing structural superpositions of NbaA (cyan) with nitrilotriacetate monooxygenase from *B. cereus* (blue; PDB code 3BPK; top), and with a putative styrene monooxygenase from *T. thermophilus* (magenta; PDB code 1USF; bottom). (D) Structure of the NbaA protomer. The N-terminal region is colored blue, the central β-barrel domain is colored cyan, and the C-terminal region is colored magenta.

Overall structure of NbaA. We found an extensive packing interaction between two neighboring molecules that were related by a crystallographic 2-fold symmetry, which was intrinsically contained in the 6_4 axis of the crystal (Fig. 1A and B). This ho-

TABLE 1 X-ray data collection and refinement statistics

Parameter	Value(s) or comment for NbaA (Cys194Ala)
Data set	
Source	BL 5C (PLS)
Wavelength (°)	0.9719
Resolution limit (°)	20–1.7
Space group	$P6_4$
Unit cell (°)	$a = 70.5, b = 70.5, c = 80.4$
Redundancy	21.6 (22.3)[a]
R_{sym} (%)	6.0 (43.4)[a]
Completeness (%)	99.5 (99.4)[a]
I/σ	92.4 (10.5)[a]
Refinement	
Resolution range (Å)	19–1.7
R factor (%)	18.8
R_{free} (%)[b]	21.6
Average B value (Å[b])	29.2
Wilsom B factor (Å[b])	23.84
RMSD for bonds (Å)	0.007
RMSD for angles (°)	1.097
Ramachandran plot	
Most favored	97.9
Additionally favored	2.1
Coordinate error (Å)	0.18
PDB code	4Z85

[a] The numbers in parentheses are statistics for the highest resolution shell.
[b] R_{free} was calculated with 5% of the data set.

modimeric assembly was consistent with previous size exclusion chromatography studies (6, 18). A similar dimeric arrangement is observed in most proteins that have structural homology to NbaA, as revealed by DALI (see Table S1) (27): a nitrilotriacetate monooxygenase from *Bacillus cereus* (PDB code 3BPK [unpublished data]); an FMN-binding enzyme from the archeaon *M. thermautotrophicum* (PDB code 1EJE [21]); a flavoredoxin from *Desulfovibrio vulgaris* (PDB code 2D5M [unpublished data]); a putative styrene monooxygenase small component from *Thermus thermophilus* (PDB code 1USF [unpublished data]); and the short-chain flavin reductase HpaC from *Sulfolobus tokodaii* (PDB code 2D37 [28]). Thus, the dimeric assembly of NbaA appears to be a common structural property of homologous proteins (Fig. 1C).

The NbaA protomer is composed of 11 β-strands and 3 α-helices (Fig. 1). The most prominent structural element of the enzyme is the seven-stranded β-barrel (β2 to β8) and two α-helices (α2 and α3), which occupy the central part (residues 24 to 166) of the primary structure of the protein. The α-helix α2 caps one end of the β-barrel, and α3 is located at the side of the β-barrel (cyan in Fig. 1D). The N- and C-terminal regions are largely extended from the central domain (blue and magenta in Fig. 1D). The N-terminal 22 residues (residues 2 to 23) are exchanged between the protomers within the homodimeric assembly, thus stabilizing the dimeric assembly. The N-terminal region contains a β-strand (β1) and one α-helix (α1). The β-strand and the α-helix form the eighth strand and cap the nonoccupied end of the β-barrel of the other protomer (Fig. 1B). The C-terminal region (residues 167 to 213) contains a paired β-strand (β9 and β10) and a β-strand (β11) on a long loop (Fig. 1B and D). The paired β-strand interacts with the β11 strand from the other subunit through the center of the 2-fold axis of the dimer, forming a β-sheet containing three β-strands (Fig. 1B).

Putative active sites of the NbaA dimer. Two large cavities were identified on the two sides of the dimer, and these cavities are surrounded by the central β-barrel and the α1 helix from the N-terminal region and the paired β-stands (β9 and β10) from the C-terminal region. A member (β4′) of the central β-strand from the other subunit is also involved in formation of the pockets (Fig. 2). The cavities did not appear to hold a ligand in the crystal structure. We assume that the occupancy of FMN might be too low to be seen in the electron density map, although the crystal looked yellow, which is an indicator of FMN binding. To analyze the role of the amino acids in the pockets, FMN was modeled in the NbaA structure based on the structure of the putative styrene monooxygenase small component from *T. thermophilus* (Fig. 2). The phosphate group of FMN was fitted into a pocket lined with Lys75, Asp106, and Glu113. However, metal ion (e.g., Mn^{2+}) coordination by the two acid residues and conformational changes of Lys75 would be required for favorable interaction with the phosphate group. In the modeled structure, the isoalloxazine ring of FMN was nicely fitted to the major part of the cavity between the β barrel and α1 (Fig. 2A). According to the binding model, the flat isoalloxazine ring is positioned almost perpendicular to the bottom surface of the cavity and is stabilized by hydrogen bonds with the backbone or side chains of Ser45, Ala46, Ala60, Val61, and Asp62 (Fig. 2B).

NbaA has been proposed to have the ping-pong bisubstrate-biproduct mechanism (6). The oxidized form of $NAD(P)^+$ leaves the binding site and is replaced by the substrate, which contacts the enzyme-bound reduced FMN. Thus, the cavity should accommodate NAD(P)H or the substrate of the enzyme in the presence of FMN, as predicted by modeling the substrate binding structures (Fig. 2). The cavity for the binding of NAD(P)H or substrate is lined with the Tyr15, Trp16, Arg25, Glu52, Asp62, Val101, Arg153, Arg187, Gly190, and Tyr193 side chains, in addition to Tyr49′, Glu52′, and Val204′ from the other subunit. Tyr15 and Tyr193 are also conserved in nitrilotriacetate monooxygenase from *B. cereus* and the putative styrene monooxygenase small component from *T. thermophilus*. These tyrosine residues may be responsible for the binding to NADPH or a substrate.

Inhibition of NbaA by 2-NBA methyl ester. In order to further obtain structural information on the substrate binding site from wild-type NbaA, the substrate-analogous inhibitor 2-NBA methyl ester was used in this study. This compound was able to inhibit ~85% of NbaA activity to 1 mM 2-NBA at 10 μM, accounting for the ratio of inhibitor to NbaA monomer of 100 to 1(Fig. 3A). The inhibition by 2-NBA methyl ester was not recovered by PD10 desalting column chromatography, indicating a strong or covalent binding of 2-NBA methyl ester to the enzyme. In contrast, ~49% of NbaA activity was inhibited by 10 μM DTNB (Table 2). 2-NBA methyl ester can inhibit NbaA enzyme activity more effectively than DTNB, which reacts with cysteine thiol(s).

In the absence of the inhibitor, the maximum NADPH oxidation rate for 2-NBA reduction by a 0.1 μM monomer concentration of NbaA in 20 mM sodium phosphate buffer (pH 7.4) was estimated to be 866 μM^{-1} min^{-1} at room temperature (Fig. 3B). Before the addition of 2-NBA, no NADPH oxidation was detected during an incubation period of 120 s. However, in the presence of 10 μM 2-NBA methyl ester, the apparent kinetic parameters,

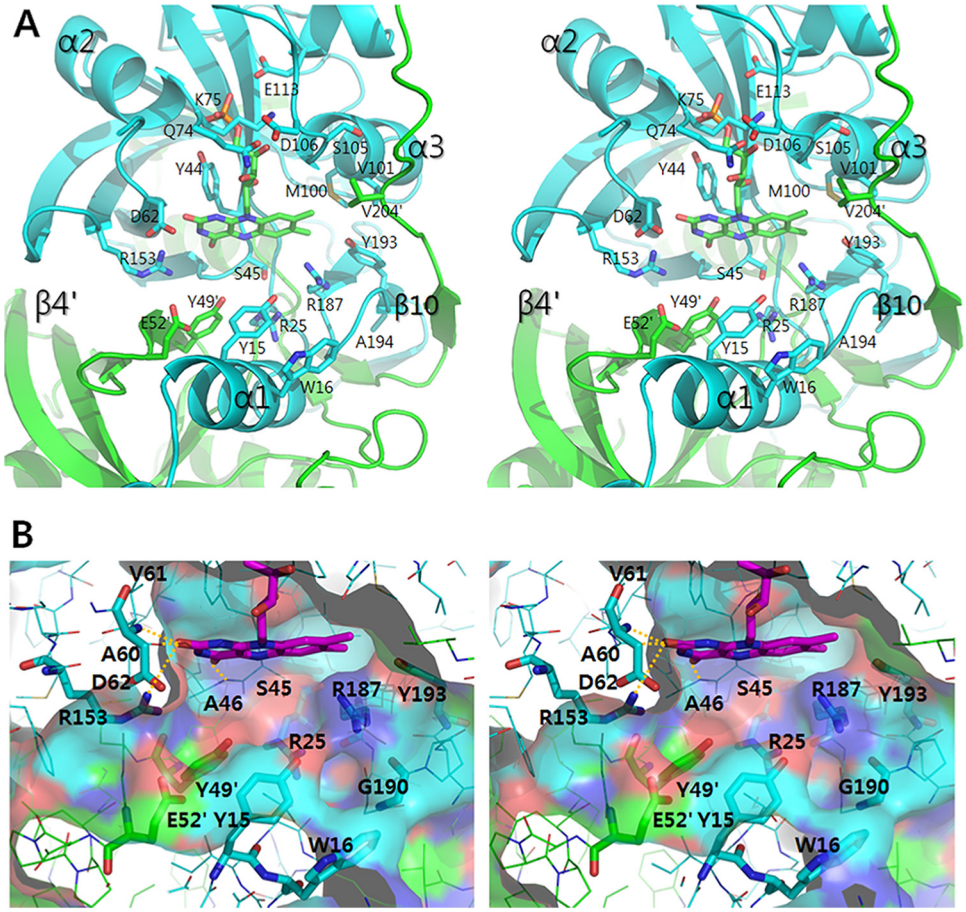

FIG 2 Cavity structures of the NbaA dimer modeled with FMN. Bound FMN was modeled based on the structural superposition with putative styrene monooxygenase from *T. thermophilus* (magenta; PDB code 1USF). The two protomers are colored cyan or green, and the modeled FMN is colored magenta. The labels of the protomer shown in green are distinguished by marks (′). (A) Stereo diagram of the central cavity of the NbaA dimer modeled with FMN. The cavity-lining residues and the putative interactions are shown in the stick representation by labels. (B) Stereo diagram of the central cavity of the NbaA dimer in the surface representation. Putative interactions with the isoalloxazine ring of the modeled FMN are shown by yellow broken lines. The residues presumed to be involved in interaction with the isoalloxazine ring of FMN, NAD(P)H, or substrates are displayed in the stick representations.

V'_{max} and K'_M, were simultaneously decreased, being similar to those in an uncompetitive inhibition. From the double-reciprocal plots shown in Fig. 3C, the inhibition constant (K_i) of 2-NBA methyl ester was determined to be 1.35 μM, which was more than 100-fold lower than the binding affinity of NbaA for 2-NBA. This phenomenon would be described by the two distinct binding-affinity states of inhibitor and substrate at the same catalytic site rather than at the two separate sites.

Mass spectrometry analysis of reactive cysteine and active site bound to 2-NBA methyl ester. A previous study showed that the Cys141 and Cys194 residues in NbaA have the potential to form intermolecular disulfide bonds that lead to enzyme inactivation under mild conditions (18). When the enzyme solution was analyzed by nondenaturing SDS-PAGE, it was difficult to distinguish between the disulfide bonding patterns whether treated or not with 1 mM 2-NBA methyl ester (Fig. 4A). We have also performed matrix-assisted laser desorption ionization–time of flight (MALDI-TOF) analysis to provide a direct evidence for chemical modification of the enzyme by the 2-NBA methyl ester; however, it was difficult to determine a shift in molecular mass due to the excess noise peaks on the baseline, probably caused by the oxidative modifications (results not shown). Because it was hard to determine the reactivity of each cysteine by gel electrophoresis and MALDI-TOF analysis, a quantitative nLC-tandem mass spectrometry method was employed to analyze disulfide-bonded peptides from tryptic digestion of the enzyme solution. The repeated analyses showed that the 2-NBA methyl ester caused a marked decrease in the formation of Cys141-Cys194 and Cys194-Cys194 disulfide bonds but did not significantly alter the levels of Cys141-Cys141 disulfide bond formation (Table 3). The representative tandem mass spectra of the three disulfide-bonded peptides are shown in Fig. S2 in the supplemental material. When the abundance of each cysteine involved in the disulfide bond formation was calculated, we found that enzyme inhibition by 2-NBA methyl ester significantly decreased the ratio of Cys194 to Cys141 in total disulfide bonds. The enzyme binding to 2-NBA methyl ester decreased the reactivity of Cys194, but not of Cys141, to form disulfide bonds.

However, tandem mass spectrometry analysis of the enzyme solution failed to identify amino acid(s) modified by 2-NBA methyl ester. In order to remove possible noise from the cysteine oxidation and disulfide bond formation, nLC-tandem mass spectrometry was performed with NbaA monomer bands (24 kDa) in

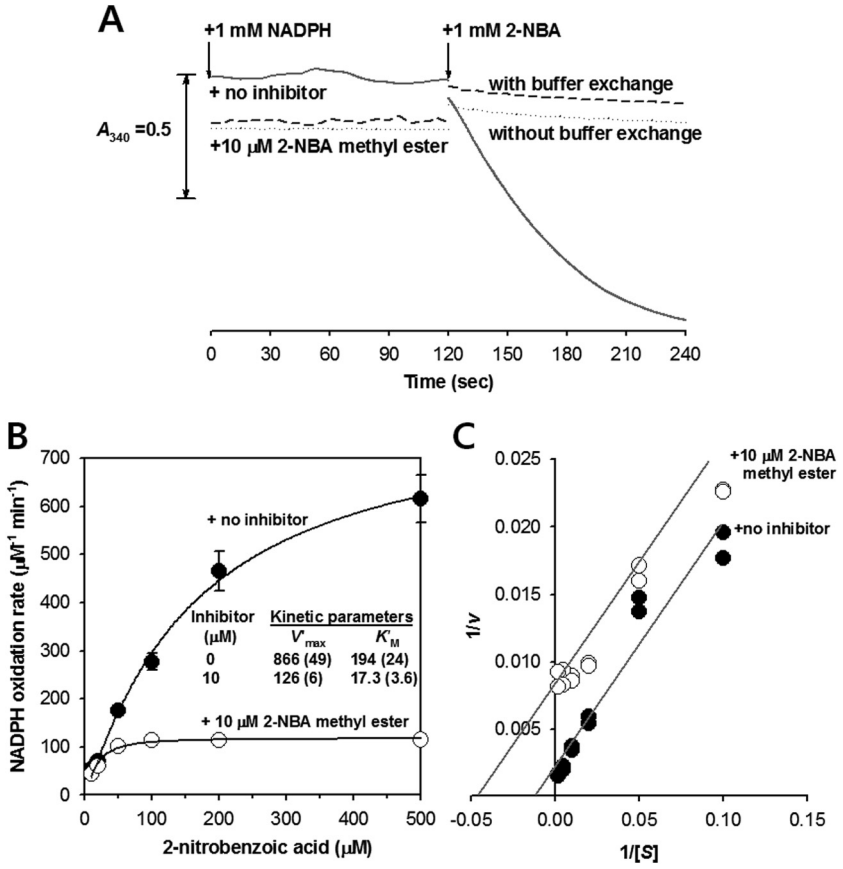

FIG 3 Oxidation of NADPH with 2-NBA substrate by NbaA in the presence or absence of 2-NBA methyl ester. (A) Time course measurements of NADPH oxidation at 340 nm before and after addition of 1 mM 2-NBA to enzyme solutions containing 0.1 μM NbaA monomer and 1 mM NADPH in 20 mM sodium phosphate, pH 7.4, untreated (solid line) or treated (dotted line) with 10 μM 2-NBA methyl ester at room temperature. A sample treated with 10 μM 2-NBA methyl ester was subjected to buffer exchange using a PD10 desalting column before the NADPH oxidation measurements (dashed line) to analyze the reversibility of enzyme inhibition. (B and C) Kinetic curves (B) and Lineweaver-Burk (C) plots of NbaA for the oxidation of NADPH with various concentrations of 2-NBA in the presence or absence of 10 μM 2-NBA methyl ester in 20 mM sodium phosphate buffer containing 0.1 μM NbaA monomer and 1 mM NADPH. Apparent kinetic parameters, V'_{max} and K'_M, in panel B were iteratively analyzed by nonlinear curve fitting to the Michaelis-Menten equation.

nondenaturing SDS-PAGE gels (Fig. 4A). Before the gel was run, the iodoacetamide modification of NbaA was carried out under nonreducing conditions to determine the reactivity of each cysteine (29). The base peak chromatograms showed that sample treated with 2-NBA methyl ester produced a different peak of *m/z* 514.6 ions with the charge state of +2 at the retention time of 80.3 min (Fig. 4B). Except for this retention time, the tandem mass spectrometry data were similar to each other (see Table S2 in the supplemental material). The collision-induced fragmentation of the *m/z* 514.6 ion produced distinct fragment ions that were matched to the tandem mass spectrum of the peptide ^{188}LGGPN Y*CR^{195}, with a 2-NBA ester bond at the asterisked Tyr193 (Y*) residue (Fig. 4C). This result showed that covalent bonding of 2-NBA methyl ester to Tyr193 decreased the iodoacetamide modification of Cys194 on the same subunit. It is possible that the bulkier residue of Tyr193 modified by 2-NBA methyl ester caused a steric hindrance or conformational change on the peptide to interfere with chymotrypsin activity on Tyr193 as well as the reactivity of Cys194. When considering the possible reaction with 2-NBA methyl ester, the Tyr193 phenol in the active site of the enzyme was presumed to be deprotonated during or prior to the transesterification reaction. Given that the carbonyl oxygen of 2-NBA methyl ester can occupy a position that functions as a general acid-base catalysis to deprotonate the Tyr193 phenol, it will disrupt the hydrogen bonding between the Tyr193 phenol and the peptide carbonyl oxygen of Leu202′ from the other subunit in

TABLE 2 Inhibitory effects of 2-nitrobenzoate methyl ester and 5,5′-dithio *bis*-(2-nitrobenzoic acid)

Inhibitor	Final concn (mM)	% activity[a]	SD
2-Nitrobenzoate methyl ester	0	100	0.1
	0.01	14.8	0.7
	0.1	2.6	5.5
	1.0	—	—
5,5′-Dithio *bis*-(2-nitrobenzoic acid)	0	100	1.3
	0.01	51.4	0.6
	0.1	14.3	1.6
	1.0	—	—

[a] One hundred percent activity represents the oxidation of 802 nmol of NADPH ml^{-1} min^{-1}, measured at a 0.1 μM monomer concentration of NbaA in 20 mM sodium phosphate buffer (pH 7.4) containing 1 mM 2-NBA, 1 mM NADPH, 1 mM DTT, 10 μM FMN, and 0.1 mM $MnCl_2$ at 25°C. Results from three independent measurements are reported as mean values and standard deviations of the means. —, not detected.

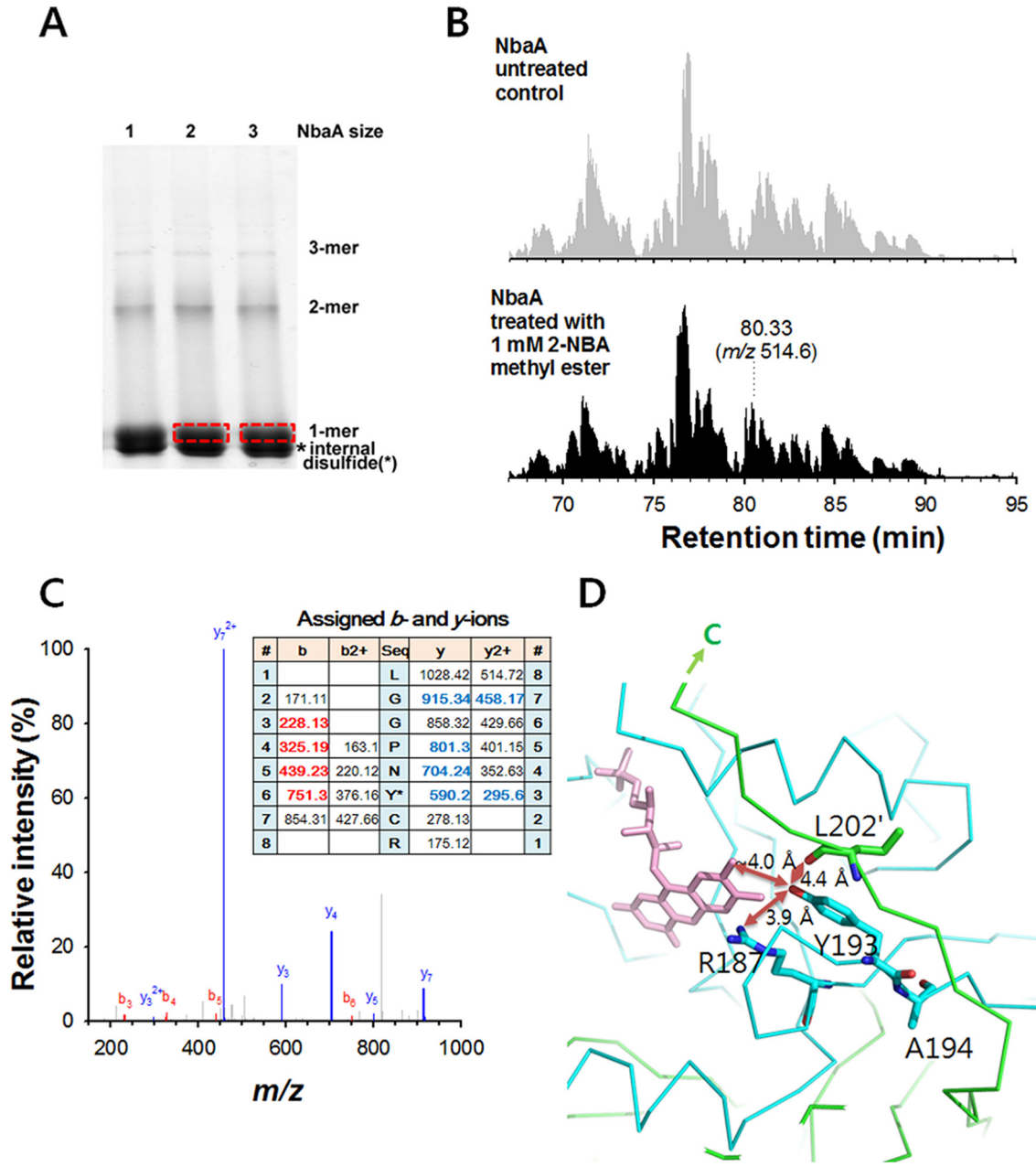

FIG 4 nLC-mass spectrometric analysis of NbaA with or without 2-NBA methyl ester. (A) Distribution patterns of NbaA monomer and high-order proteins corresponding to the sizes of dimers and trimers in a nondenaturing SDS-PAGE gel. After FMN reconstitution, purified protein was preincubated with or without 1 mM 2-NBA methyl ester and then treated with 10 mM iodoacetamide in 20 mM sodium phosphate buffer (pH 7.4) at room temperature prior to gel separation. NbaA monomer bands in red boxes were excised from the gel and used for the analysis by nLC-tandem mass spectrometry, as described in Materials and Methods. Lanes: 1, FMN-free NbaA; 2 and 3, FMN-bound NbaA untreated (2) and treated (3) with 1 mM 2-NBA methyl ester. (B) Base-peak chromatograms of NbaA monomers left untreated (top) or treated (bottom) with 2-NBA methyl ester. Treatment with 2-NBA methyl ester resulted in a significantly different peak of *m/z* 514.6 ion with the charge state of +2 at the retention time of 80.33 min. (C) The tandem mass spectrum of the *m/z* 514 ion, assigned to the predicted *b*- and *y*-ions generated from collision-induced dissociation of the peptide ^{188}LGGPNY*CR^{195}, which contains a 2-NBA ester bond at the asterisked Tyr193 (Y*) position. (D) The environment surrounding Tyr193 and Ala194. In this structure, Cys194 was replaced with an alanine residue. Tyr193 and its adjacent residue are located on a β-strand (β10). The side chain of Tyr193 orientates toward the central cavity, whereas the side chain of Ala194 (or Cys194) is positioned in the opposite direction. If a compound with a bulky nonpolar group modifies Tyr193, the binding of FMN is hampered and/or the Ala194 (or Cys194 in the wild-type enzyme) might be less accessible to the solvent.

the C-terminal loop, as shown in the structure model of NabA (Fig. 4D). Thus, the Tyr193 modification has potential to cause a change not only in the local environment of the adjacent Cys194, but also in the catalytic site of NbaA.

Site-directed mutation of Tyr193 to phenylalanine abolishes FMN binding to NbaA. In the structure of the Cys194Ala NbaA variant, Tyr193 is located in the putative FMN binding site. The most similar proteins, such as an FMN-binding protein MTH152

TABLE 3 Effects of 2-NBA methyl ester on the formation of disulfide bonds at the Cys141 and Cys194 residues in the wild-type NbaA protein[a]

Disulfide bonds	Value for:	
	Untreated control	Treated with 2-NBA methyl ester
Cys141-Cys141	39.5 ± 2.1	36.0 ± 1.4
Cys141-Cys194	21.0 ± 1.4	13.5 ± 0.7**
Cys194-Cys194	29.5 ± 2.1	17.5 ± 2.1**
Cys194/Cys141ratio	0.80 ± 0.02	0.56 ± 0.08**

[a] One microgram of FMN-reconstituted NbaA protein, untreated or treated with 1 mM 2-NBA methyl ester in 20 mM sodium phosphate solution (pH 7.4), was used for two independent analyses by nLC-tandem mass spectrometry, as described in Materials and Methods. Representative tandem mass spectra of the identified peptides with disulfide bonds at the Cys141 and Cys194 residues are shown in Fig. S2 in the supplemental material. Statistical differences between the treated and untreated samples were analyzed by Student's *t* test: **, $P < 0.01$.

(PDB code 1EJE) of *M. thermautotrophicum* (21), a flavin reductase component PheA2 (PDB code 1RZ1) of *B. thermoglucosidasius* A7 (30), a styrene monooxygenase (PDB code 1USF), and a probable flavoprotein (PDB code 1WGB) of *T. thermophilus* (unpublished data), contain the hydrophobic tyrosine and phenylalanine residues in the conserved flavin-binding sites. To elicit the functional group of Tyr193 in NbaA, this residue was replaced with structurally conserved phenylalanine by site-directed mutagenesis. When analyzed by nLC-tandem mass spectrometry, the Tyr193Phe NbaA mutant was found to contain no unique peptide modified by 2-NBA methyl ester (see Table S2). This supported that the Tyr193 residue was the modification site for 2-NBA methyl ester.

The Tyr193Phe mutants of both the wild-type NbaA and the Cys194Ala mutant resulted in the fast dissociation of FMN from gel filtration and hence abolished the catalytic activity (Table 4; see also Fig. S3 in the supplemental material). There was no significant difference in the stoichiometry of FMN binding to the wild-type NbaA and Cys194Ala mutant proteins within a range of 0.32 to 0.36, although there were evident differences in the kinetic parameters for NADPH-dependent 2-NBA reduction. Their FMN binding abilities were significantly reduced at baseline after treatment with 1 mM 2-NBA methyl ester (see Fig. S3). During gel filtration, it was possible to dissociate FMN from the protein, so the FMN stoichiometry might be underestimated. We have attempted to estimate equilibrium constants for the FMN binding to the apoproteins purified by the phenyl-Sepharose chromatography followed by the buffer exchanges using PD10 desalting columns; however, the concentrations of FMN bound to the wild-type NbaA and Cys194Ala mutant proteins largely varied within a micromolar range of concentrations in solution and declined over time to below the detection limit by an hour with the addition of less than 10 μM FMN under ambient atmospheric conditions (data not shown), possibly owing to the inhibitory effects of the residual salts and/or the formation of disulfide bonds under the reconstitution conditions, as previously described for the enzyme assay (18). Thus, gel filtration despite the problem (during which FMN will dissociate) was used to remove the negative effects on FMN binding and isolate the FMN-bound dimers. Although the observed stoichiometry depends on the conditions of gel filtration, it was useful in this study for distinguishing the effects of 2-NBA methyl ester, Tyr193Phe mutant, and Cys194Ala mutant on the inhibition of FMN binding. This also supported that modification of the Cys194 thiol plays a critical role in regulating the allosteric inhibition of NbaA, as described previously (18). The partial binding of FMN to the wild-type NbaA and Cys194Ala mutant proteins explains why it was difficult to analyze the crystals complexed with FMN.

The mutant studies suggest that the Tyr193 hydroxyl group, but not the Cys194 thiol group, may play an essential role in the FMN-binding site of the NbaA dimer. It is consistent with the observation that covalent binding of the 2-NBA methyl ester to Tyr193 inhibits NbaA irreversibly by the release of FMN from the protein, as demonstrated by the disappearance of yellow color from the crystal of the FMN-reconstituted Cys194Ala variant treated with 1 mM 2-NBA methyl ester (see Fig. S1 in the supplemental material). In addition to oxidative modification, modifi-

TABLE 4 Stoichiometry of FMN binding to wild-type and mutant NbaA proteins and kinetic parameters for NADPH-dependent 2-nitrobenzoate reduction

Protein	Stoichiometry of FMN binding[a]	Apparent kinetic parameters for NADPH-dependent 2-nitrobenzoate reduction[b]		
		V'_{max} (μM min^{-1})	K'_M (μM)	k_{cat} (min^{-1})
Wild-type NbaA				
+ no inhibitor	0.361 ± 0.005	866 ± 49	194 ± 24	4.49 ± 0.29
+ 1 mM 2-NBA methyl ester	ND	ND	ND	ND
Cys194Ala				
+ no inhibitor	0.324 ± 0.084	298 ± 15*	345 ± 28*	1.15 ± 0.04*
+ 1 mM 2-NBA methyl ester	ND	ND	ND	ND
Tyr193Phe	0.100 ± 0.004***	ND	ND	ND
Tyr193Phe-Cys194Ala	0.106 ± 0.001**	ND	ND	ND

[a] Statistically significant differences in the stoichiometry of FMN binding to Tyr193Phe and Tyr193Phe-Cys194Ala mutants compared to wild-type NbaA are shown, determined by two-tailed *t* tests, with the significance shown as follows: **, $P < 0.01$, and ***, $P < 0.001$.

[b] The apparent kinetic parameters, V'_{max} for NADPH oxidation and K'_M for 2-NBA, were analyzed using a 0.1 μM monomer concentration of gel-filtered proteins, as described in the legend to Fig. 3B. Statistically significant differences in kinetic parameters of Cys194Ala mutant compared to wild-type NbaA are shown, as determined by two-tailed *t* tests, with the significance shown as follows: *, $P < 0.05$. ND, not detected.

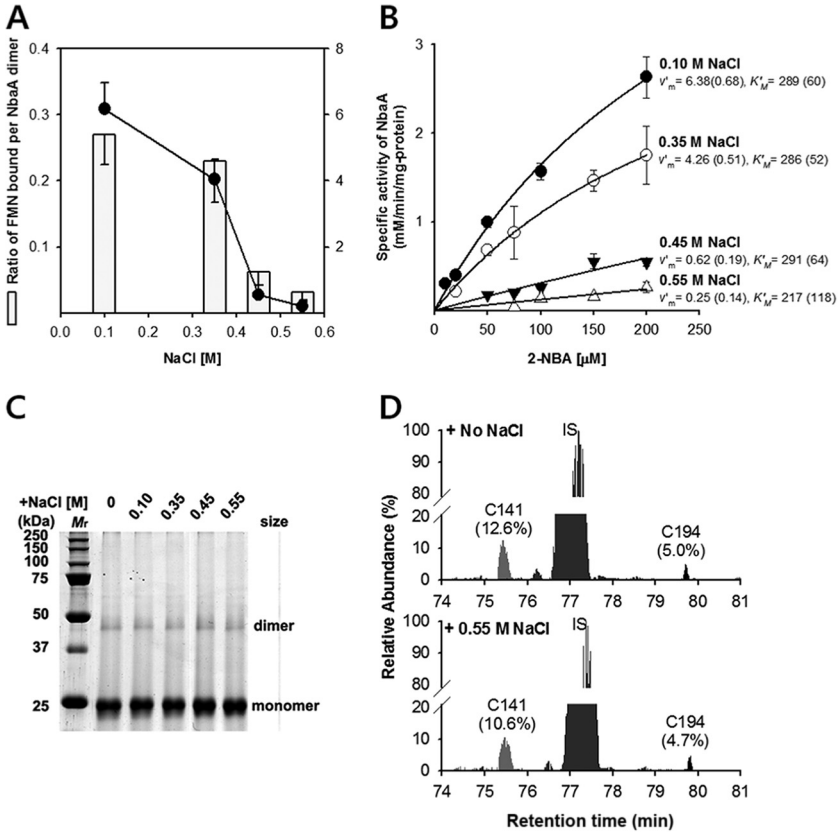

FIG 5 Effects of NaCl concentration on FMN content and cysteine reactivity of NbaA. (A) Negative effect of NaCl concentration on FMN content and enzymatic activity of NbaA. The ratio of FMN bound per NbaA dimer was determined by a spectrophotometric method, as described in Materials and Methods. Specific activity of FMN-reconstituted NbaA for NADPH oxidation at a 0.1 μM monomer concentration of NbaA was measured in ambient conditions by the addition of 1 mM 2-NBA and 1 mM NADPH to 20 mM sodium phosphate buffer (pH 7.4) with the same concentrations of NaCl as used in FMN reconstitution. (B) Kinetic curves of NbaA reconstituted with FMN at 0.1 M, 0.35 M, 0.45 M, and 0.55 M NaCl. Specific activity of FMN-reconstituted NbaA was determined with various concentrations of 2-NBA in the presence of 1 mM NADPH in 20 mM sodium phosphate buffer (pH 7.4) with the same concentrations of NaCl as used in FMN reconstitution. Each plot of the observed NADPH oxidation rate (v') versus 2-NBA concentration [S] was fitted to a hyperbolic function, $v' = v'_m \times [S]/(K'_M + [S])$, and the apparent maximum rate (v'_m) of NADPH oxidation and Michaelis-Menten constant (K'_M) for 2-NBA are shown as mean values, with standard errors in parentheses at the right of each curve. (C) Disulfide-bonding pattern of FMN-reconstituted NbaA at 0.1 M, 0.35 M, 0.45 M, and 0.55 M NaCl. After PD10 column elution using 20 mM sodium phosphate buffer (pH 7.4) with the same NaCl concentrations, 2.5 μg of the eluted protein was treated with 10 mM iodoacetamide at room temperature for 1 h before analysis by nondenaturing SDS-PAGE and visualization by silver staining. (D) Extracted ion chromatograms (XICs) of reactive cysteine-containing peptides, ^{132}ITDAPIAWEC#K^{142} (C141, m/z = 652.54, z = +2) and ^{188}LGGPNYC#R^{195} (C194, m/z = 469.02, z = +2), containing iodoacetamide modifications (C#) of Cys141 and Cys194 in 0.55 M NaCl-treated (bottom) and untreated (top) samples. The XICs were analyzed from the nLC-mass spectrometry data with a mass tolerance of 100 ppm and normalized to the relative abundance of an unmodified peptide, DLTPSTTIDVPR (m/z = 658.15, z = +2), used as an internal standard (IS) expressed as 100%.

cation of the Tyr193 hydroxyl group presents a new regulatory mechanism for the inhibition of NbaA that can occur even in the environment where the reactivity of Cys194 is reduced. Accordingly, modifications of Tyr193 and Cys194 residues located at the juxtaposition of the active-site cavity and the C-terminal loop, respectively, represent alternative mechanisms for regulating NbaA enzyme activity under reducing and oxidizing conditions.

NaCl concentration affects FMN content but not cysteine reactivity. The above data suggested that modification of the Tyr193 hydroxyl group had negative effects on FMN binding and the Cys194 reactivity of NbaA. However, it was unclear whether the FMN content influences the reactivity of Cys194. To examine this effect, the FMN content of wild-type NbaA was varied by the addition of 0.1 M, 0.35 M, 0.45 M, or 0.55 M NaCl to the enzyme solution at pH 7.4. As a consequence, the FMN content was markedly decreased by high NaCl concentrations at or above 0.35 M NaCl, showing a correlation with the specific activity of NbaA toward 2-NBA (Fig. 5A). The increased NaCl concentration decreased the apparent maximum reaction rate without apparent change in the substrate binding affinity of the enzyme (Fig. 5B). This change indicated that NbaA and its substrate complex were equally inhibited by NaCl in a noncompetitive manner. Despite some discrepancies in the inhibition mode, the lowered FMN content of NbaA was similar to those seen with the Tyr193Phe mutant and the 2-NBA methyl ester.

The enzyme treated with various concentrations of NaCl did not significantly change the disulfide bonding patterns (Fig. 5C). When the NbaA monomer bands at 0 and 0.55 M NaCl were analyzed by nLC-mass spectrometry, there were no significant differences in the extracted ion chromatograms of carbamidomethyl cysteine (indicated by C#) Cys141- and Cys194-containing peptides, ^{132}ITDAPIAWEC#K^{142} and ^{188}LGGPNYC#R^{195}, which were normalized to the intensity of an unmodified peptide, DLT PSTTIDVPR, expressed as 100% (Fig. 5D). Although the mass

spectrometry had higher ionization efficiency for the Cys141-containing peptide than for the Cys194-containing peptide, the constant ratios of Cys141 and Cys194 indicated that NaCl concentration did not affect the cysteine reactivity of NbaA. These results suggest that the decreased content of FMN *per se* does not affect the reactivity of Cys194. It was different from the inhibition by 2-NBA methyl ester, which reduced the reactivity of Cys194 as well as the binding of FMN to the NbaA dimer. As below discussed, a chemical modification of the Tyr193 hydroxyl group with a bulky nonpolar group like that of the 2-NBA methyl ester can deteriorate the hydrogen bonding network in the FMN binding site of the NbaA dimer, presumably inducing a steric hindrance or conformational change which perturbs the reactivity of Cys194 on the protein surface.

DISCUSSION

NbaA from *P. fluorescens* KU-7 is a unique enzyme with the specificity to reduce 2-NBA to 2-hydroxylaminobenzoate, and it shows altered substrate specificity toward 2,4-dinitrobenzoate during the formation of intermolecular disulfide bonds between Cys141 and Cys194 residues under oxidative stress conditions *in vitro* and by stimulating ROS generation in the recombinant *E. coli* cells (17, 18). On the basis of its structural and biochemical properties, it is classified into a family of flavin-binding reductases (protein family PF03358). Despite extensive efforts, the crystal structure of NbaA has not yet been solved due to distortion of the crystal even in the presence of a reducing agent in solution. This seems to be because of the strong propensity to form intermolecular disulfide bonds between Cys141 and Cys194 residues, thereby resulting in the formation of high-order proteins that interfere with crystallization. Although the Cys141 residue is conserved in other flavin reductase proteins, Cys194 appears not to be conserved. Therefore, a Cys194Ala mutant was used to obtain the structure model of NbaA, even though the two cysteine-to-alanine mutations (Cys141Ala and Cys194Ala) have similar levels of effectiveness in reducing the extent and progression of the disulfide bond formation without loss of enzyme activity (18). Although the double cysteine-to-alanine mutant at positions 141 and 194 is considered more effective in preventing the disulfide bond formation, it is not suited as a structure model of NbaA because it lacks enzyme activity (18). The protein structure and activity of NbaA may be changed by modifications of the Cys141 and Cys194 residues.

Cysteine oxidation is a crucial mechanism for the regulation of enzyme activity by influencing the protein structure (31, 32). Under a relatively mild oxidative condition at the physiological pH, Cys141 and Cys194 are oxidized to form disulfide bonds, which are readily reduced by the induced production of thioredoxin A (TrxA) in *E. coli* (17). In the cells, disulfide bond formation protects proteins from the oxidation of cysteine thiol and sulfenic acid to sulfinic acid, sulfonic acid, and other cysteine derivatives in high oxidation states which cannot be reduced by major cellular reductants, such as glutathione and thioredoxin (33). It is interesting that covalent binding of 2-NBA methyl ester to Tyr193 in the active site of NbaA reduces the reactivity of Cys194 on the protein surface. According to the functional categories of Marino and Gladyshev (34), Cys141 and Cys194 are classified as regulatory cysteines that serve as posttranslational modification sites for the regulation of enzyme. However, the function of Cys194 cannot be determined unambiguously in the presence of the substrate-analog inhibitor, which reduces the reactivity of Cys194 but does not affect the reactivity of Cys141. There is no canonical sequence motif to classify all categories of the functional cysteine that is affected by exposure to solvent or electrostatic interaction with polar groups in the vicinity and/or exposure to a different solvation environment compared to an aqueous solution (35, 36). An exposed cysteine is significantly more polar than a buried one as a result of interaction with the solvent either on the molecular surface or in the solvated polar microenvironment of protein pockets and cavities (34, 35). In the structure model of the NbaA dimer, Tyr193 and Cys194 are located on a β10 strand, in which the side chain of Tyr193 orientates toward the central cavity, whereas the side chain of Cys194 is positioned in the opposite direction. The Cys194 thiol groups are laid on the protein surface, either exposed or buried, and face each other through the interprotomer interactions mediated by hydrogen bonding between the paired β-strand loop and the central cavity. In this structure, an oxidative modification of Cys194 can disrupt the hydrogen bond network surrounding the cavity, resulting in distorted protein conformation and leading to the release of FMN from protein as well as the formation of intermolecular disulfide bonds between the two reactive cysteine residues at Cys141 and Cys194. This study suggests that both of the modified Tyr193 and Cys194 residues in the oxidizing and reducing environments result in inactivation of NbaA activity via the loss of FMN. The disulfide bond formation of NbaA is a reversible inactivation process that is readily reverted in the reducing environment of the cytoplasm by redox proteins, such as *E. coli* thioredoxin A (17), which may potentially allow the reduced dimer to recover the original activity by reincorporation of FMN. Under this condition, although the reactivity of Cys194 for oxidative modification is lowered, a chemical modification of Tyr193 by a bulky nonpolar molecule has the potential of acting as a counterregulator of NbaA activity via an irreversible inactivation of the enzyme by the loss of FMN.

Several nitroaromatic reductases from *E. coli* and *Enterobacter cloacae* have been complexed with substrate analogs, inhibitors, and dinitrobenzoate prodrugs that were stacked above the isoalloxazine ring of FMN (31, 32, 37). These complexes are useful for predicting the FMN binding pocket and the substrate binding site on the basis of the NbaA structure model. The tertiary structure of NbaA consists of a central domain and the extended N- and C-terminal regions (Fig. 1D). The N- and C-terminal regions function as arms to support homodimer formation as the catalytic form, a feature shared with other homologous proteins. From the modeled structure (Fig. 2), the isoalloxazine ring of FMN is well positioned in the active-site cavity surrounded by the central β-barrel, the α1 helix from the N-terminal region, and the paired β-stands (β9 and β10) from the C-terminal loop region. In earlier work (18), truncation of the C-terminal loop (residues 194 to 216) abolished NbaA enzyme activity, suggesting that the C-terminal loop is essential in maintaining the protein structure and function. In the presence of FMN, the two substrates, NADPH and 2-NBA, are possibly accommodated within the active-site cavity via a ping-pong mechanism. In the transition state model of the enzyme-substrate complex, the 2-nitro group of 2-NBA is predicted to sit on the N5 atom of FMN by electrostatic interaction with the side chain of Arg187 (6). This orientation assists in stabilization of the substrate binding pocket, which might accommodate the 1-carboxylate anion of 2-NBA by a salt bridge with the side chain of Arg153 and hydrogen bonds with Tyr15 and Tyr49′ from the

other subunit. These side chain interactions may be responsible for the substrate specificity of NbaA.

Mass spectrometry revealed that NbaA was inactivated by the covalent bonding of the substrate-analogous 2-NBA methyl ester with Tyr193. Because the normal tyrosine nucleophile is too weak to attack the carbonyl carbon of the ester via a transesterification process, it should be deprotonated either prior to or after the reaction with 2-NBA methyl ester. The activated hydroxyl group of Tyr193 will facilitate the transesterification reaction of the 2-NBA methyl ester, because it is energetically favored to form the nucleophile attacking the carbonyl carbon atom through general base catalysis (38). In general, the carbonyl bond (C=O) of the ester is shorter than that of the amide, so the carbonyl bond of 2-NBA methyl ester should be brought into proximity of the Tyr193 hydroxyl group prior to the reaction. The structural data show that Tyr193 makes van der Waals contact with the hydrophobic dimethylbenzene of FMN and hydrogen bonding with the guanidinium group of Arg187 and the peptide carbonyl oxygen of Leu202′ from the other subunit (Fig. 4D). Site-directed mutagenesis showed that the Tyr193 hydroxyl group is essential for the binding of FMN to protein. Together, these findings show that this residue not only is essential in the FMN binding site but also contributes to polar interactions with other functional groups in the cavity and the C-terminal loop from the other subunit. Hence, its binding to the 2-NBA methyl ester can break the hydrogen bond, likely affecting the acid dissociation constant (pK_a) of nearby groups in the catalytic site (39). It is similar to the effect of NaCl concentration that decreases the FMN content of the NbaA dimer seemingly by a decrease in electrostatic interactions. Given that the putative substrate binding model of NbaA is compatible with binding of the substrate-analogous 2-NBA methyl ester, the substrate binding pocket for the 1-carboxylate anion of 2-NBA is likely destabilized by the binding of 2-NBA methyl ester without negative charge, which will cause a change in the dielectric constant of the cavity to decrease the pK_a value of Tyr193.

In conclusion, we demonstrated that modifications of Tyr193 and Cys194 residues in NbaA are important not only for determining the protein structure and function but also for understanding the dynamic control mechanism of the enzyme. There is increasing interest in reactive cysteine residues that significantly influence protein structure and activity in nearly all organisms (40–44). Despite the tremendous increase in the number of known redox-regulated proteins, there are still many unknown factors that influence the reactivity of cysteine in the native protein. Quantitative LC-tandem mass spectrometric profiling of reactive cysteine of the native protein is useful for the characterization of cysteine reactivity (29) and, in combination with structural and biochemical data, provides a new strategy for the identification of functional groups by covalent bonding with amino acid-specific reagents (45). In this study, the substrate-analogous inhibitor 2-NBA methyl ester provided useful structural and mechanistic insights into the catalytic site of NbaA. Posttranslational modifications of Tyr193 and Cys194 residues located in the active-site cavity and the C-terminal loop represent alternative mechanisms for the regulation of NbaA in reducing as well as in oxidizing environments.

ACKNOWLEDGMENTS

This research was supported by the Research Resettlement Fund for the new faculty of Seoul National University to N.-C.H. and by the Basic Science Research Program (2013R1A1A2060761 to Y.-H.K.) and Research Fellow Program (2014R1A1A2005424 to W.S.) through the National Research Foundation (NRF) of Korea, funded by the Ministry of Education.

REFERENCES

1. **Cenas N, Prast S, Nivinskas H, Sarlauskas J, Arnér ESJ.** 2006. Interactions of nitroaromatic compounds with the mammalian selenoprotein thioredoxin reductase and the relation to induction of apoptosis in human cancer cells. J Biol Chem **281:**5593–5603.
2. **Spain JC.** 1995. Biodegradation of nitroaromatic compounds. Annu Rev Microbiol **49:**523–555. http://dx.doi.org/10.1146/annurev.mi.49.100195.002515.
3. **Ju KS, Parales RE.** 2010. Nitroaromatic compounds, from synthesis to biodegradation. Microbiol Mol Biol Rev **74:**250–272. http://dx.doi.org/10.1128/MMBR.00006-10.
4. **Khan H, Harris RJ, Barna T, Craig DH, Bruce NC, Munro AW, Moody PCE, Scrutton NS.** 2002. Kinetic and structural basis of reactivity of pentaerythritol tetranitrate reductase with NADPH, 2-cyclohexenone, nitroesters, and nitroaromatic explosives. J Biol Chem **277:**21906–21912. http://dx.doi.org/10.1074/jbc.M200637200.
5. **Cain RB.** 1958. The microbial metabolism of nitro-aromatic compounds. J Gen Microbiol **19:**1–14. http://dx.doi.org/10.1099/00221287-19-1-1.
6. **Iwaki H, Muraki T, Ishihara S, Hasegawa Y, Rankin KN, Sulea T, Boyd J, Lau PCK.** 2007. Characterization of a pseudomonad 2-nitrobenzoate nitroreductase and its catabolic pathway-associated 2-hydroxylaminobenzoate mutase and a chemoreceptor involved in 2-nitrobenzoate chemotaxis. J Bacteriol **189:**3502–3514. http://dx.doi.org/10.1128/JB.01098-06.
7. **Muraki T, Taki M, Hasegawa Y, Iwaki H, Lau PCK.** 2003. Prokaryotic homologs of the eukaryotic 3-hydroxyanthranilate 3,4-dioxygenase and 2-amino-3-carboxymuconate-6-semialdehyde decarboxylase in the 2-nitrobenzoate degradation pathway of *Pseudomonas fluorescens* strain KU-7. Appl Environ Microbiol **69:**1564–1572. http://dx.doi.org/10.1128/AEM.69.3.1564-1572.2003.
8. **Takenaka S, Murakami S, Kim YJ, Aoki K.** 2000. Complete nucleotide sequence and functional analysis of the genes for 2-aminophenol metabolism from *Pseudomonas* sp. AP-3. Arch Microbiol **174:**265–272. http://dx.doi.org/10.1007/s002030000203.
9. **Hughes MA, Williams PA.** 2001. Cloning and characterization of the *pnb* genes, encoding enzymes for 4-nitrobenzoate catabolism in *Pseudomonas putida* TW3. J Bacteriol **183:**1225–1232. http://dx.doi.org/10.1128/JB.183.4.1225-1232.2001.
10. **Providenti MA, Shaye RE, Lynes KD, McKenna NT, O'Brien JM, Rosolen S, Wyndham RC, Lambert IB.** 2006. The locus coding for the 3-nitrobenzoate dioxygenase of *Comamonas* sp. strain JS46 is flanked by IS*1071* elements and is subject to deletion and inversion events. Appl Environ Microbiol **72:**2651–2660. http://dx.doi.org/10.1128/AEM.72.4.2651-2660.2006.
11. **Hasegawa Y, Muraki T, Tokuyama T, Iwaki H, Tatsuno M, Lau PCK.** 2000. A novel degradative pathway of 2-nitrobenzoate via 3-hydroxyanthranilate in *Pseudomonas fluorescens* strain KU-7. FEMS Microbiol Lett **190:**185–190. http://dx.doi.org/10.1111/j.1574-6968.2000.tb09284.x.
12. **Pandey G, Paul D, Jain RK.** 2003. Branching of *o*-nitrobenzoate degradation pathway in *Arthrobacter protophormiae* RKJ100: identification of new intermediates. FEMS Microbiol Lett **229:**231–236. http://dx.doi.org/10.1016/S0378-1097(03)00844-9.
13. **Dantzer R, O'Connor JC, Freund GG, Johnson RW, Kelley KW.** 2008. From inflammation to sickness and depression: when the immune system subjugates the brain. Nat Rev Neurosci **9:**46–56. http://dx.doi.org/10.1038/nrn2297.
14. **Delpech B.** 2014. Formation and reactivity of 5-aminopenta-2,4-dienals: useful intermediates for nitrogen heterocycles synthesis. Adv Heterocycl Chem **111:**1–41.
15. **Todd WP, Carpenter BK, Schwarcz R.** 1989. Preparation of 4-halo-3-hydroxyanthranilates and demonstration of their inhibition of 3-hydroxyanthranilate oxygenase activity in rat and human brain tissue. Prep Biochem **19:**155–165.
16. **Linderberg M, Hellberg S, Björk S, Gotthammar B, Högberg T, Persson**

K, Schwarcz R, Luthman J, Johansson R. 1999. Synthesis and QSAR of substituted 3-hydroxyanthranilic acid derivatives as inhibitors of 3-hydroxyanthranilic acid dioxygenase (3-HAO). Eur J Med Chem **34:**729–744. http://dx.doi.org/10.1016/S0223-5234(99)00220-2.

17. **Kim YH, Yu MH.** 2012. Overexpression of reactive cysteine-containing 2-nitrobenzoate nitroreductase (NbaA) and its mutants alters the sensitivity of *Escherichia coli* to reactive oxygen species by reprogramming a regulatory network of disulfide-bonded proteins. J Proteome Res **11:**3219–3230. http://dx.doi.org/10.1021/pr300221b.
18. **Kim YH, Song WS, Go H, Cha CJ, Lee C, Yu MH, Lau PCK, Lee K.** 2013. 2-Nitrobenzoate 2-nitroreductase (NbaA) switches its substrate specificity from 2-nitrobenzoic acid to 2,4-dinitrobenzoic acid under oxidizing conditions. J Bacteriol **195:**180–192. http://dx.doi.org/10.1128/JB.02016-12.
19. **Otwinosky Z, Minor W.** 1997. Processing of X-ray diffraction data collected in oscillation mode. Methods Enzymol **276:**307–326.
20. **Collaborative Computational Project, Number 4.** 1994. The CCP4 suite: programs for protein crystallography. Acta Crystallogr **D50:**760–763.
21. **Christendat D, Yee A, Dharamsi A, Kluger Y, Savchenko A, Cort JR, Booth V, Mackereth CD, Saridakis V, Ekiel I, Kozlov G, Maxwell KL, Wu N, McIntosh LP, Gehring K, Kennedy MA, Davidson AR, Pai EF, Gerstein M, Edwards AM, Arrowsmith CH.** 2000. Structural proteomics of an archaeon. Nat Struct Biol **7:**903–909. http://dx.doi.org/10.1038/82823.
22. **Emsley P, Cowtan K.** 2004. Coot: model-building tools for molecular graphics. Acta Crystallogr D **60:**2126–2132. http://dx.doi.org/10.1107/S0907444904019158.
23. **Adams PD, Grosse-Kunstleve RW, Hung LW, Ioerger TR, McCoy AJ, Moriarty NW, Read RJ, Sacchettini JC, Sauter NK, Terwilliger TC.** 2002. PHENIX: building new software for automated crystallographic structure determination. Acta Crystallogr D **58:**1948–1954. http://dx.doi.org/10.1107/S0907444902016657.
24. **Aliverti A, Curti B, Vanoni MA.** 1999. Identifying and quantitating FAD and FMN in simple and in iron-sulfur-containing flavoproteins. Methods Mol Biol **131:**9–23.
25. **Hinkson JW.** 1968. *Azotobacter* free-radical flavoprotein: preparation and properties of the apoprotein. Biochemistry **7:**2666–2672. http://dx.doi.org/10.1021/bi00847a033.
26. **Yoon BY, Kim YH, Kim N, Yun BY, Kim JS, Lee JH, Cho HS, Lee K, Ha NC.** 2013. Crystal structure of the periplasmic copper binding protein CueP from *Salmonella enterica* serovar Typhimurium. Acta Crystallogr D **69:**1867–1875.
27. **Holm L, Sander C.** 1993. Protein structure comparison by alignment of distance matrices. J Mol Biol **233:**123–138. http://dx.doi.org/10.1006/jmbi.1993.1489.
28. **Okai M, Kudo N, Lee WC, Kamo M, Nagata K, Tanokura M.** 2006. Crystal structures of the short-chain flavin reductase HpaC from *Sulfolobus tokodaii* strain 7 in its three states: $NAD(P)^+$-free, NAD^+-bound, and $NADP^+$-bound. Biochemistry **45:**5103–5110. http://dx.doi.org/10.1021/bi052313i.
29. **Weerapana E, Wang C, Simon GM, Richter F, Khare S, Dillon MBD, Bachovchin DA, Mowen K, Baker D, Cravatt BF.** 2010. Quantitative reactivity profiling predicts functional cysteines in proteomes. Nature **468:**790–795. http://dx.doi.org/10.1038/nature09472.
30. **van den Heuvel RHH, Westphal AH, Heck AJR, Walsh MA, Rovida S, van Berkel WJH, Mattevi A.** 2004. Structural studies on flavin reductase PheA2 reveal binding of NAD in an unusual folded conformation and support novel mechanism of action. J Biol Chem **279:**12860–12867. http://dx.doi.org/10.1074/jbc.M313765200.
31. **Haynes CA, Koder RL, Miller AF, Rodgers DW.** 2002. Structures of nitroreductases in three states: effects of inhibitor binding and reduction. J Biol Chem **277:**11513–11520. http://dx.doi.org/10.1074/jbc.M111334200.
32. **Johansson E, Parkinson GN, Denny WA, Neidle S.** 2003. Studies on the nitroreductase prodrug-activating system: crystal structures of complexes with the inhibitor dicoumarol and dinitrobenzamide prodrugs and of the enzyme active form. J Med Chem **46:**4009–4020. http://dx.doi.org/10.1021/jm030843b.
33. **Klomsiri C, Karplus PA, Poole LB.** 2011. Cysteine-based redox switches in enzymes. Antioxid Redox Signal **14:**1065–1077. http://dx.doi.org/10.1089/ars.2010.3376.
34. **Marino SM, Gladyshev VN.** 2012. Analysis and functional prediction of reactive cysteine residues. J Biol Chem **287:**4419–4425. http://dx.doi.org/10.1074/jbc.R111.275578.
35. **Britto PJ, Knipling L, Wolff J.** 2002. The local electrostatic environment determines cysteine reactivity of tubulin. J Biol Chem **277:**29018–29027. http://dx.doi.org/10.1074/jbc.M204263200.
36. **Roos G, Foloppe N, Messens J.** 2013. Understanding the pK_a of redox cysteines: the key role of hydrogen bonding. Antioxid Redox Signal **18:**94–127. http://dx.doi.org/10.1089/ars.2012.4521.
37. **Lovering AL, Hyde EI, Searle PF, White SA.** 2001. The structure of *Escherichia coli* nitroreductase complexed with nicotinic acid: three crystal forms at 1.7 Å, 1.8 Å and 2.4 Å resolution. J Mol Biol **309:**203–213. http://dx.doi.org/10.1006/jmbi.2001.4653.
38. **Ilieva S, Atanasov Y, Galabov B.** 2008. Mechanism of the aminolysis of phenyl acetate: a computational study. Bulg Chem Commun (Camb) **40:**401–408.
39. **Harris TK, Turner GJ.** 2002. Structural basis of perturbed p$K_a$values of catalytic groups in enzyme active sites. IUBMB Life **53:**85–98. http://dx.doi.org/10.1080/15216540211468.
40. **Eichler J, Adams MWW.** 2005. Posttranslational protein modification in *Archaea*. Microbiol Mol Biol Rev **69:**393–425. http://dx.doi.org/10.1128/MMBR.69.3.393-425.2005.
41. **Foyer CH, Noctor G.** 2005. Redox homeostasis and antioxidant signaling: a metabolic interface between stress perception and physiological responses. Plant Cell **17:**1866–1875. http://dx.doi.org/10.1105/tpc.105.033589.
42. **Brandes N, Schmitt S, Jakob U.** 2009. Thiol-based redox switches in eukaryotic proteins. Antioxid Redox Signal **11:**997–1014. http://dx.doi.org/10.1089/ars.2008.2285.
43. **Jortzik E, Wang L, Becker K.** 2012. Thiol-based posttranslational modifications in parasites. Antioxid Redox Signal **17:**657–673. http://dx.doi.org/10.1089/ars.2011.4266.
44. **Lindahl M, Mata-Cabana A, Kieselbach T.** 2011. The disulfide proteome and other reactive cysteine proteomes: analysis and functional significance. Antioxid Redox Signal **14:**2581–2642. http://dx.doi.org/10.1089/ars.2010.3551.
45. **Mendoza VL, Vachet RW.** 2009. Probing protein structure by amino acid-specific covalent labeling and mass spectrometry. Mass Spectrom Rev **28:**785–815. http://dx.doi.org/10.1002/mas.20203.